

Article

Macroscopic Behavior and Microscopic Factors of Electron Emission from Chained Nanocarbon Coatings

Daleri Boqizoda *, Anatoly Zatsepin, Evgeny Buntov, Anatoly Slesarev, Daria Osheva and Tatiana Kitayeva

Institute of Physics and Technology, Ural Federal University, Mira st. 21, 620002 Ekaterinburg, Russia

* Correspondence: bobot92@mail.ru

Received: 30 July 2019; Accepted: 30 August 2019; Published: 9 September 2019



Abstract: The carbyne-containing films based on linear-chain carbon are promising materials for the manufacture of electronic equipment components. These carbyne-containing materials can be used as active elements of computational electronics and as ultra-miniature sensors of gaseous environment. The temperature studies of the electrical characteristics of carbyne-containing films by most of the scientific groups are limited to the low temperature range in which the quantum properties of nanostructures are most pronounced. We studied carbyne-containing films with a thickness of 20 and 400 nm on copper and silicon substrates using optically stimulated electron emission (OSEE) in the temperature range from room temperature (RT) to 400 °C. Theoretical modeling explains the dependence of work function on termination groups and substrate lattice. Experimental data revealed a relationship between the spectral characteristics of electron emission and temperature. The spectral contributions of both surface states and bulk interband transitions were clearly distinguishable.

Keywords: carbyne; chained structures; ab initio; DFT; electron emission; work function; electronic properties

1. Introduction

Carbon materials have formed an interesting area of materials science research in recent decades. Of particular interest are the low-dimensional carbon modifications—nanodiamonds, graphene, fullerenes, and nanotubes. Their unique features and applications in various fields, from biology to nanoelectronics, have attracted the attention of researchers. Investigations of 1D-materials with chains were also performed, although they remain unappreciated, particularly carbyne [1–3], due to the restrictions in synthetic methods.

Microcrystalline carbyne with dimensions of about 100 nm were acquired by thermal annealing [4] in the 1960s. Although many methods have been proposed for the synthesis of carbyne, amorphous or poorly ordered films/powders with a crystallite size less than 100 nm were obtained. In order to obtain more defined films, a robust and reliable characterization technique must be selected. Widely spread optical spectroscopy techniques are complicated or not suitable for opaque samples and layered structures. As a result, the information available on the surface layer of functional materials, particularly amorphous, is incomplete and is usually obtained by numerical modeling techniques. The experimental characterization of the surface states in nanostructures, both intrinsic and defect- or adsorbate-related, is an important task [5,6].

In this article, we use optically stimulated electron spectroscopy (OSEE) in combination with ab initio modeling, which allowed us to reveal the influence of temperature, thickness, and substrate type on the band structure and low vacuum photoemission threshold of linear-chained carbon

(LCC)-containing coatings. Earlier experimental results on OSEE of silicon- and copper-based chains were described in our recent paper [7]. The modeling aimed to interpret the emission properties on substrate type, while thermal issues were addressed experimentally.

2. Samples and Methods

Linear-chained carbon (LCC) films, 20 nm and 400 nm in thickness, were grown on polycrystalline copper and monocrystalline silicon substrates by ion-stimulated condensation from a carbon plasma in a narrow window of optimal parameters [8]. The custom experimental setup for LCC films deposition (Ekaterinburg, Russia) was a vacuum system that provided pulsed carbon ion beam from a carbon plasma with a density of 10^{13} – 10^{14} cm^{-3} and an ionization degree of 95%. The pulse rate varied in the range 1–30 Hz and the pulse duration was of the order of 100 microseconds. The growth of the film was stimulated by additional irradiation with Ar^+ ions. The ion beam was formed by a source of low-pressure ions. The energy of the Ar^+ bombarding the surface of the growing film was in the range 0–500 eV and depended on the extraction voltage and on the parameters of the carbon plasma. The working pressure in the vacuum chamber was 10^{-4} Pa.

The ASED electron spectrometer (Figure 1, Ekaterinburg, Russia) made it possible to measure the electron emission spectral response in the temperature interval of 20–400 °C. Contrary to stationary external photoelectron emission and internal photoinjection currents over interface barriers, the OSEE is a nonstationary photoelectron emission from localized surface-near electronic states into vacuum [9]. The spectra obtained in our experiments were normalized against the source light flux. The spectral position error for described setup was less than 0.03 eV while the intensity error did not exceed 5%. Additional error caused by OSEE nonstationarity, which was lower than registered background intensity and two–three orders below than measured signal. The obtained nonselective spectral dependences were processed using original “OSEE-fitter” software [10], implementing the models described below.

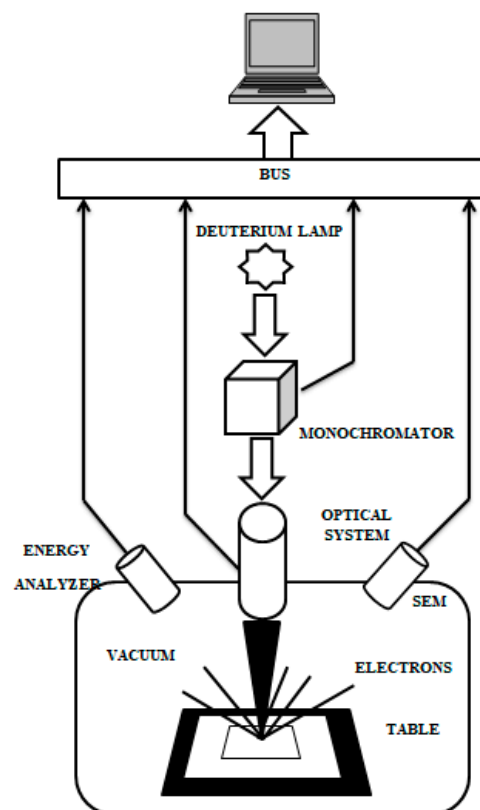


Figure 1. Scheme of the optically stimulated electron spectroscopy (OSEE) spectrometer. UV light is focused on the sample surface, which emits electrons registered by electron multiplier.

The Copper (111) slab has been optimized using CASTEP code with Perdew-Burke-Ernzerhof (PBE) pseudopotential in generalized gradient approximation (GGA), taking into account surface relaxation. The silicon (111)- $\sqrt{3} \times \sqrt{3}$ surface model has been taken from [11]. Consequently, the 12 atom-long carbon chains with kinks were placed on top of slabs, forming 2D hexagonal lattices. The graphical representations of the model under study can be found in our work [7]. Final geometry optimization was performed before the properties calculation. The same models and settings were applied to calculate the electric potential along the z-axis, perpendicular to the slab surface. Work functions were calculated as a difference between Fermi energy and the vacuum potential 10 nm away from the surface.

3. Results and Discussion

3.1. OSEE Measurements

Here, we use the Kane dependence to study linear-chained carbon films on copper and silicon substrates with different thicknesses. The Kane power law [12] reflects the high-energy part of OSEE spectra (5 eV to 5.7 eV, Figure 2), which we attribute to optical transitions between surface states with subsequent thermal release to vacuum:

$$I = A(h\nu - \Phi)^n \quad (1)$$

where A is a magnitude fitting parameter, Φ is the photoelectric work function, and n is the power factor, which indicates the governing type of interband electron transitions [13].

The parameters of OSEE curves fitted by Equation (1) are shown in Table 1. The n factor values were found between 2 and 3, showing that the electron emission was related to both direct and indirect optical transitions. Considering a significant error in parameter determination, all this experimental data may be matched to model values. Thin films of linear-chain carbon exhibited a stable value of n around 2.7 over the entire temperature range. This implies that the electron emission was mainly due to the indirect transitions between surface energy states with the participation of phonon processes. From Table 1, the value of Φ varies from 4.0 to 4.5 eV for samples of films with a thickness of 400 nm, while the value is less by 0.1–0.2 eV for films with a thickness of 20 nm.

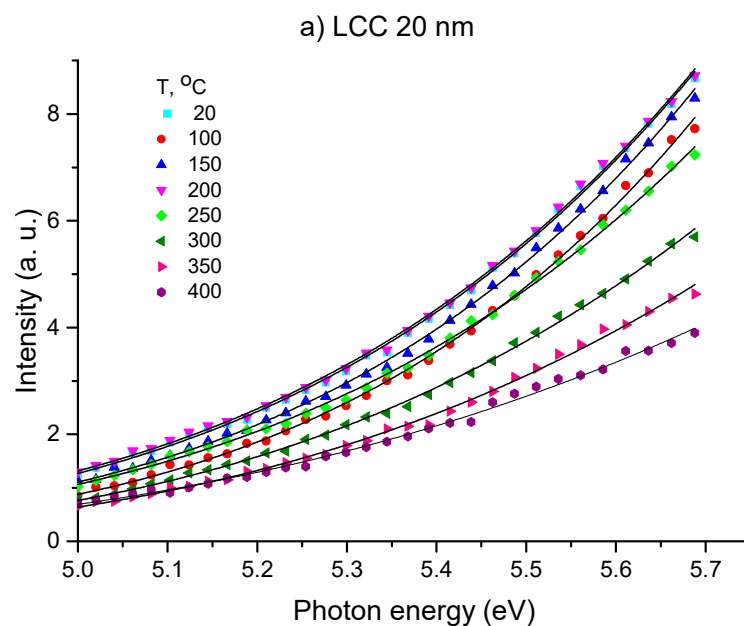


Figure 2. Cont.

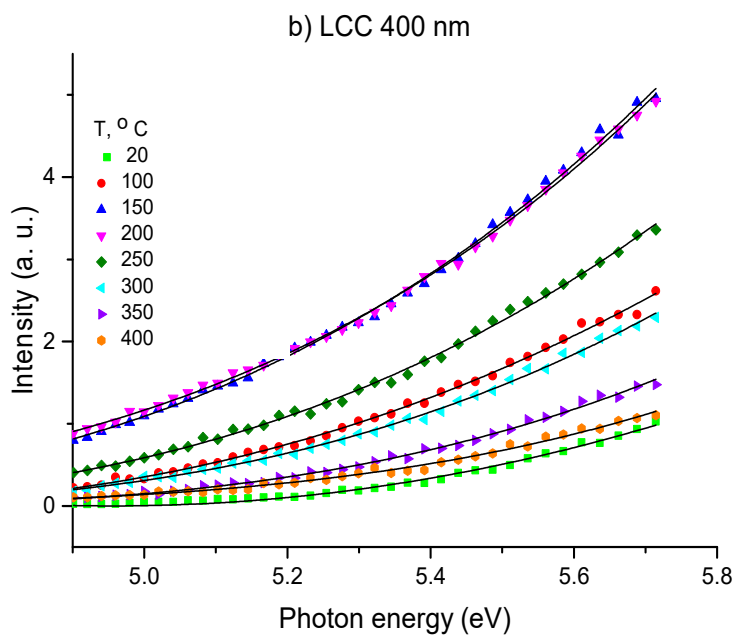


Figure 2. Approximation of the high-energy part of the OSEE spectra for carbyne-containing films with a thickness of 20 nm (a) and 400 nm (b) on a copper substrate using the Kane equation.

Table 1. Kane parameters for OSEE of the samples under study.

Temperature, °C	LCC 20 nm Φ , eV	LCC 400 nm Φ , eV
20	4.26	4.50
100	4.14	4.53
150	4.36	4.03
200	4.30	4.03
250	4.24	4.19
300	4.35	4.27
350	4.47	4.47
400	4.10	4.47

A good fit between experiment and Equation (1) was achieved both for silicon- and copper-based samples. The quality of the carbon coating on the surface of crystalline silicon was better than on copper. Furthermore, the variation of the work function caused by the film was insignificant [7]. In other words, in this case, the electrons were emitted from the carbon layer only. In contrast, the copper plate itself had lower work function and, therefore, the electrons emitted from the holes in the inhomogeneous film dominated in the total intensity of the OSEE, so no changes were registered with increasing thickness of the carbon layer. Limited spatial resolution of ultraviolet photoelectron emission made the micron landscape of the carbon coating inaccessible.

As evidenced by the results of [7] and the current paper, the optically stimulated electron emission of the carbyne-containing films demonstrate poor dependence of the work function on the film thickness. From the Figure 2, the anomalous temperature dependence, with a maximum intensity achieved at 450–500 K, can be observed. On the one hand, the corresponding thermal energy may give rise to the low-frequency vibrations around 350 cm^{-1} present in the Raman spectra [7]. Alternatively, this temperature region corresponds to the predicted conversion of cumulene chains to polyene form [14]. Understanding of the electron emission features requires the elaboration of the microscopic mechanism behind. Despite a complex nanocomposite structure of the coating under study, we started our numerical investigations with an idealized model of short chains on crystalline substrate.

3.2. Density-Functional Theory (DFT) Modeling

In order to discover the reasons of the work function change in the samples under study, we performed the DFT calculation of the electric potential along the axis perpendicular to the substrate. Surface slabs of copper crystal cut by (001), (110), and (111) planes were covered by a layer of carbon chains (Figure 3a).

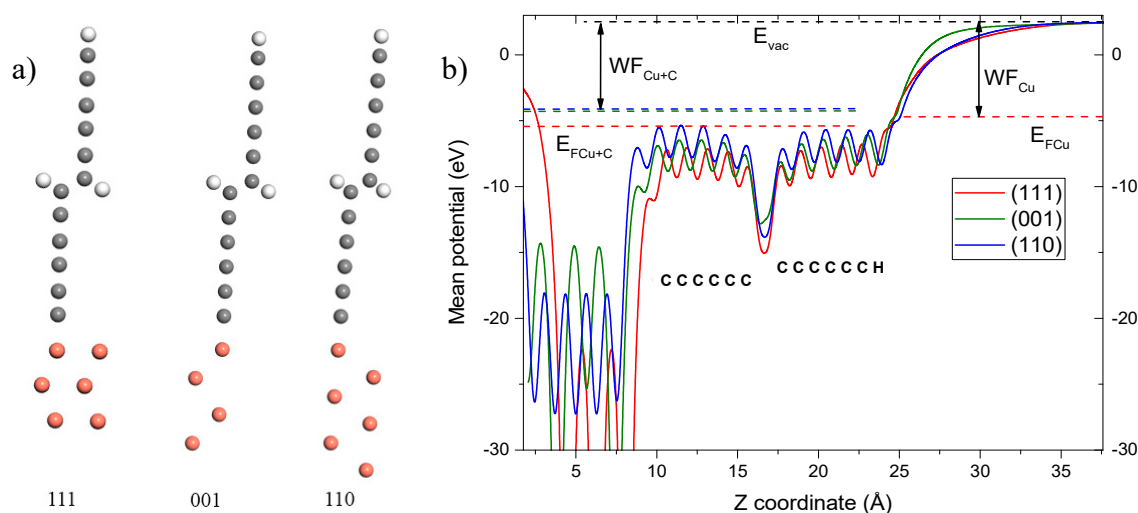


Figure 3. (a) Structural models of copper substrate with chains before structural relaxation (brown dots are copper atoms, gray carbon atoms, and lighter hydrogen); (b) Estimated potential chart for linear-chained carbon (LCC)-coated films for different subsystems. Fermi levels are shown by dashed lines, work functions are indicated by arrows. The position of the carbon and hydrogen atoms in the chains can be found in the lower diagram.

Figure 3b shows the spatial distribution of the average electric potential along the Z axis, normal to the surface. The left part of the graph shows the potential along the copper substrate, the potential along the carbon chain is shown from 7 Å. The right part, from 25 Å, corresponds to the vacuum layer. The difference between the vacuum level and the Fermi level in this system allowed us to obtain the thermodynamic work function. When calculated this way, the theoretical work function calculated depends on the crystalline orientation of the substrate and is comparable with the literature data for pure copper [13]. The magnitude of the work function slightly depends on the type of substrate (Table 2), the highest value corresponds to (111) plane.

Table 2. The values of work function depending on the orientation of the substrate.

Orientation of the substrate	Φ_{theor} , eV [10]	E_F , eV	E_{vacuum} , eV	Φ_{theor} , eV (calculated)
(111)	7.7	5.4	2.52	7.92
(001)	8.0	4.4	2.52	6.92
(110)	6.8	4.3	2.52	6.82

The main obstacle for the bottom-up synthesis of carbon chains is their high reactivity, and therefore, their inclination to crosslink and change to a more stable carbon modification [15,16]. This challenge even made scientists neglect the possible existence of a carbyne allotrope. The passivating terminal groups, which are aimed to cap the most reactive sites, play a crucial role in preventing the crosslink.

Therefore, in our study, the carbon chains with hydrogen atoms at the bend and with terminal groups of CH, CH₂, and CH₃ were placed on top of the Si 111 substrate (Figure 4a). The chains were arranged in such a way that a hexagonal structure with an interchain distance of about 5 Å was formed. Images of the spatial distribution of electronic orbitals are presented in Figure 4a. It can be seen how their shape depends on the type of end group, reflecting the charge redistribution.

Author Contributions: Numerical calculations—D.O., T.K.; OSEE experiments—A.S.; writing—original draft preparation, D.B.; writing—review and editing—E.B., A.Z.

Funding: The work was carried out in the laboratory “Functional Materials Physics for Carbon Micro- and Optoelectronics” and supported by Act 211 Government of the Russian Federation, contract № 02.A03.21.0006 and in part by the Ministry of Education and Science of the Russian Federation (Government Task No. 3.1485.2017/4.6).

Conflicts of Interest: The authors declare no conflict of interest.

References

1. Mingjie, L. Carbyne from first principles: Chain of C atoms, a nanorod or a nanorope. *ACS Nano* **2013**, *7*, 10075–100082.
2. Christopher, B.; Goldman, N. Carbyne fiber synthesis within evaporating metallic liquid carbon. *J. Phy. Chem. C* **2015**, *119*, 21605–21611.
3. Bitao, P. Carbyne with finite length: The one-dimensional sp carbon. *Sci. Adv.* **2015**, *1*, e1500857.
4. Sladkov, A.M.; Kasatochkin, V.I.; Korshak, V.V. New crystalline form of carbon - carbyne. USSR Patent No. 107, 7 December 1971. Priority date 4 November 1960.
5. Pacchioni, G.; Skuja, L.; Griscom, D. *Defects in SiO₂ and Related Dielectrics: Science and Technology*; Springer: Heidelberg, Germany, 2012; p. 624.
6. Luth, H. Solid Surfaces. In *Interfaces and Thin Films*; Springer: Heidelberg, Germany, 2010; p. 586.
7. Buntov, E.A.; Zatsepin, A.F.; Slesarev, A.I.; Shchapova, Y.V.; Challinger, S.; Baikie, I. Effect of thickness and substrate type on the structure and low vacuum photoemission of carbyne-containing films. *Carbon* **2019**, *152*, 388–395. [[CrossRef](#)]
8. Kudryavtsev, Y.P.; Guseva, M.B.; Babaev, V.G. Oriented carbyne layers. *Carbon* **1992**, *30*, 213–221. [[CrossRef](#)]
9. Zatsepin, A.F.; Biryukov, D.Y.; Kortov, V.S. Taking account of the nonstationarity in analyzing the optically stimulated electron emission of irradiated dielectrics. *J. Appl. Spectr.* **2005**, *72*, 671–678. [[CrossRef](#)]
10. Buntov, E.A.; Zatsepin, A.F. OSEE fitter program, registered in the Russian state register of software. No. 2008614289. 11 November 2008.
11. Smeu, M.; Guo, H.; Ji, W.; Wolkow, R.A. Electronic properties of Si(111)-7 × 7 and related reconstructions: Density functional theory calculations. *Phys. Rev. B* **2012**, *85*, 195315. [[CrossRef](#)]
12. Kane, E.O. Theory of Photoelectric Emission from Semiconductors. *Phys. Rev.* **1962**, *127*, 131. [[CrossRef](#)]
13. Anderson, P.A. The Work Function of Copper. *Phys. Rev.* **1949**, *76*, 388–390. [[CrossRef](#)]
14. Wong, C.H.; Buntov, E.A.; Rychkov, V.N.; Guseva, M.B.; Zatsepin, A.F. Simulation of chemical bond distributions and phase transformation in carbon chains. *Carbon* **2017**, *114*, 106–110. [[CrossRef](#)]
15. Ravagnan, L.; Siviero, F.; Lenardi, C.; Piseri, P.; Barborini, E.; Milani, P.; Casari, C.S.; Li Bassi, A.; Bottani, C.E. Cluster-beam deposition and in situ characterization of carbyne-rich carbon films. *Phys. Rev. Lett.* **2002**, *89*, 285506. [[CrossRef](#)]
16. Lucotti, A.; Casari, C.S.; Tommasini, M.; Li Bassi, A.; Fazzi, D.; Russo, V.; Del Zoppo, M.; Castiglioni, C.; Cataldo, F.; Bottani, C.E.; et al. Sp Carbon chain interaction with silver nanoparticles probed by Surface Enhanced Raman Scattering. *Chem. Phys. Lett.* **2009**, *478*, 45. [[CrossRef](#)]
17. Casari, C.S.; Milani, A. Carbyne: From the elusive allotrope to stable carbon atom wires. *MRS Commun.* **2018**, *8*, 207–219. [[CrossRef](#)]
18. Allen, F.G.; Cobelli, G.W. Work Function, Photoelectric Threshold and Surface States of Atomically Clean Silicon. *Phys. Rev.* **1962**, *127*, 150–158. [[CrossRef](#)]



© 2019 by the authors. Licensee MDPI, Basel, Switzerland. This article is an open access article distributed under the terms and conditions of the Creative Commons Attribution (CC BY) license (<http://creativecommons.org/licenses/by/4.0/>).